JOURNAL OF MATERIALS SCIENCE 33 (1998) 969–975

Characterization of yttria-stabilized zirconia thin films deposited by electron beam evaporation on silicon substrates

M. HARTMANOVÁ, I. THURZO, M. JERGEL, J. BARTOŠ
Institute of Physics, Slovak Academy of Sciences, 84228 Bratislava, Slovakia
E-mail: fyzihart@savba.sk

F. KADLEC, V. ZELEZNÝ
Institute of Physics, Czech Academy of Sciences, 18040 Prague, Czech Republic

D. TUNEGA
Institute of Inorganic Chemistry, Slovak Academy of Sciences, 84236 Bratislava, Slovakia

F. KUNDRACIK
Department of Physics, Faculty of Mathematics and Physics, Comenius University, 84215 Bratislava, Slovakia

S. CHROMIK
Institute of Electrical Engineering, Slovak Academy of Sciences, 84239 Bratislava, Slovakia

M. BRUNEL
Laboratoire de Cristallographie du CNRS, 38042 Grenoble, France

Structure, phase composition and electrical conductivity of thin yttria-stabilized zirconia (YSZ) films deposited by electron beam evaporation on a silicon (1 0 0) substrate at different temperatures i.e. room temperature (r.t.), 700 and 830 °C, as well as the quality of the YSZ–Si interface have been investigated. The phase composition was verified by Raman spectroscopy and by infrared (i.r.) transmission measurements. The structure of films changed in agreement with their electrical conductivity depending on the deposition temperature. Both structure and thereby electrical conductivity were influenced by the high concentration of Y_2O_3 stabilizer used and by the post-deposition thermal treatment of films. The deposition temperature was also important in determining the quality of the YSZ–Si interface and hence the accessible sweep of the surface potential. The capacitance–voltage characteristics of the metal–insulator–semiconductor (MIS) structures incorporating YSZ films measured at r.t. showed hysteresis and positive shifts of the flat-band voltages.

1. Introduction

Thin film electrolytes are interesting for their technological applications in fuel cells [1], sensors [2] and electrochemical devices [3]. Different deposition techniques are suitable for the production of such materials. In the present work, electron beam evaporation of zirconia thin films is used. The properties of the film, especially the phase composition and structure, which are strongly related to ionic conductivity, depend on the parameters of deposition.

Mixed oxide systems like stabilized zirconia, are of particular interest from this point of view. The ionic conductivity of zirconia based electrolytes depends on the structure, the microstructure and the impurity level of the zirconia [4–6]. Crystallographic ordering is controlled by the amount of stabilizing oxide, the deposition parameters and the thermal post-deposition treatment of the films.

In this paper the main results of the structure, phase composition and electrical conductivity of YSZ thin films deposited by electron beam evaporation on Si substrates, as well as the quality of the YSZ–Si interface, are reviewed and discussed with special regard to the preparation conditions, namely the temperature of deposition (or the temperature of the substrate).

2. Experimental procedure

2.1. Characterization of films

YSZ films were deposited on n-doped Si (1 0 0) substrates by electron beam evaporation of $(YO_{1.5})_{0.18}(ZrO_2)_{0.82}$ pellets. The respective temperatures of the substrate were r.t., 700 and 830 °C. The deposition rate of 0.1 nm s^{-1} yielded a typical thickness for YSZ of 100 nm, measured using Talystep

(Taylor–Hobson) equipment. The details of the preparation can be found in [7, 8].

2.2. Experimental methods

2.2.1. X-ray diffraction (XRD)

XRD was studied in in-plane grazing-incidence asymmetric geometry with CuK_α radiation, a graphite monochromator being placed in the primary-beam path. A 12 kW Rigaku rotating-anode generator and a 120° wide-angle position sensitive Inel detector were used. Three different angles of incidence, 0.5, 0.8 and 1.5°, were chosen.

2.2.2. Unpolarized Raman spectra

Raman spectra were analysed on a Jeol-JRS-S1 spectrophotometer (double-grating monochromator and photon-counting system). The 488 nm line of the Ar laser was used as an exciting line. All spectra were measured in right-angle scattering geometry at r.t.

2.2.3. I.R. transmission spectra

These were measured in the range 50–4000 cm^{-1} using a Bruker IFS-113v Fourier-transform spectrometer. A spectral resolution of 2 cm^{-1} was used and the spectra were smoothed in order to remove interference oscillations from the substrate.

2.2.4. Electrical conductivity

This was measured by a complex impedance method in air. A Solartron 1260 frequency response analyser was used in the frequency range 10 Hz–1 MHz. The experimental apparatus was interfaced with a computer in order to process the data.

Aluminium dots (0.34 mm^2) were evaporated on the YSZ film through a metal mask from a tungsten boat at 10^{-4} Pa. A large area Au ohmic contact was also evaporated on the back side (Si) of the sandwich configuration (MIS structure of the type Al–YSZ–Si–Au).

The cell constant of the deposition films, $K = l/S$, where S was the surface area and l, the thickness, was estimated within $\pm 10\%$ of its average value. The measurements of the temperature dependence of conductivity (150–560 °C) for each deposition temperature were repeated five times.

2.2.5. Charge deep-level transient spectroscopy (DLTS) and feedback charge capacitance–voltage (C–V) measurements

These were performed by means of a versatile time-domain spectrometer that enabled the switching between DLTS and feedback charge capacitance modes [9].

3. Results and discussion

3.1. Structural evolution

The phase composition of deposited YSZ films is sensitively dependent on the deposition temperature, i.e. the temperature of the substrate (Fig. 1a–c), the composition changing from essentially amorphous YSZ at r.t. (Fig. 1a) through the best developed cubic fluorite-type structure, face centred cubic (f.c.c.) at 700 °C (Fig. 1b) to a cubic phase combined with an amorphous one at 830 °C (Fig. 1c). There is no evidence for the presence of tetragonal or monoclinic zirconia.

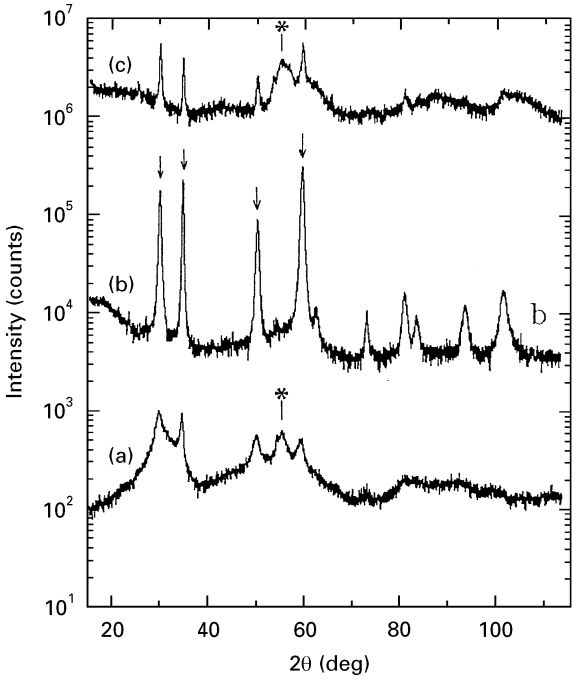

Figure 1 X-ray diffraction patterns from YSZ films deposited on Si substrate as a function of deposition temperature: (a) r.t., (b) 700 °C, and (c) 830 °C; the curves (b) and (c) are shifted upwards by a factor of 50 and 10^4, respectively. The maxima labelled by the arrows are 1 1 1, 2 0 0, 2 2 0 and 3 1 1 reflections of cubic fluorite-type structure; the modulation (*) comes from the Si substrate (grazing angle 0.8°).

The structure of the film deposited at r.t. was mostly amorphous, a crystalline phase started to form but did not progress further (see the weak diffraction peaks in Fig. 1a). No changes in the diffraction patterns of the films were seen with an increasing angle of incident X-rays. This meant that whatever the structure, it was always homogeneous across the thin film.

The best developed f.c.c. structure was found to occur at a deposition temperature of 700 °C. The XRD pattern at this temperature shows, as can be seen in Fig. 1b, four sharp peaks that are assigned to the reflections from the 1 1 1, 2 0 0, 2 2 0 and 3 1 1 planes of cubic YSZ.

The lattice parameter a_0, and the average grain size, D, were determined from the 2 0 0 peaks ($2\Theta = 34.56$) in the XRD pattern obtained at 700 °C. The lattice parameter, $a_0 = 0.5184$ nm did not change with the deposition temperature. An increase of the lattice parameter by 2% in comparison with the reference ZrO_2 phase from the PDF-2 database was found.

The average grain size, $\bar{D} = 24.5$ nm, was determined using the Scherrer [10] equation

$$\bar{D} = k\lambda/\beta \cos\Theta \quad (1)$$

where $\bar{D}$ was the average grain size; k a constant close to unity; λ the wavelength of the X-ray source; Θ the Bragg angle of the peak used in the determination,

i.e. 2 0 0; and $\beta = 2\Delta\Theta$, $\Delta\Theta$ being the full-width at half-maximum (FWHM) in radians of a Bragg maximum. We put $k = 1$ and took into account the experimental resolution $\Delta\Theta_{exp} = 0.08$, supposing the Gaussian profile too.

The content of the f.c.c. phase in the film deposited at 830 °C decreased compared with that of the film deposited at a temperature of 700 °C (Fig. 1b, c). This can be judged from the decrease of intensity of the Bragg maxima; the average grain size, $\bar{D}$ is approximately the same as for the deposition at 700 °C. Moreover, an amorphous phase is apparent, probably due to the surface "softening" of the substrate at a deposition temperature of 830 °C. This amorphous phase is qualitatively different from that formed at r.t. It seems (see the conductivity measurements) that in spite of some amorphous phase apparent at 830 °C, the density of this film is higher than that relevant to 700 °C; this is in agreement with the known behaviour of YSZ.

No interfacial products and no zirconate phases, which were expected to increase the interfacial resistance, were detected neither before the electrical measurements nor after the five repeated measurements. However, the high concentration of the stabilizer used (~30 mol % Y_2O_3 or ~20 mol % $YO_{1.5}$) caused partial precipitation of yttria before electrical measurements (Fig. 2).

Repeated measurements of conductivity, i.e. following five repeated cycles of sample heating and cooling (r.t.–560 °C), have an effect on the structure of the film as well as on its electrical conductivity. As can be seen in Fig. 3, the f.c.c. structure of the film deposited at r.t. is much better developed after such post-deposition thermal treatment of the sample. The average grain size, $\bar{D}$ was determined to be 10.8 nm in this case. The opposite effect of such thermal treatment was observed for the film deposited at 830 °C (Fig. 2). Only weak 1 1 1, 2 2 0 and 3 1 1 reflections from the f.c.c. structure and stronger reflections from the secondary

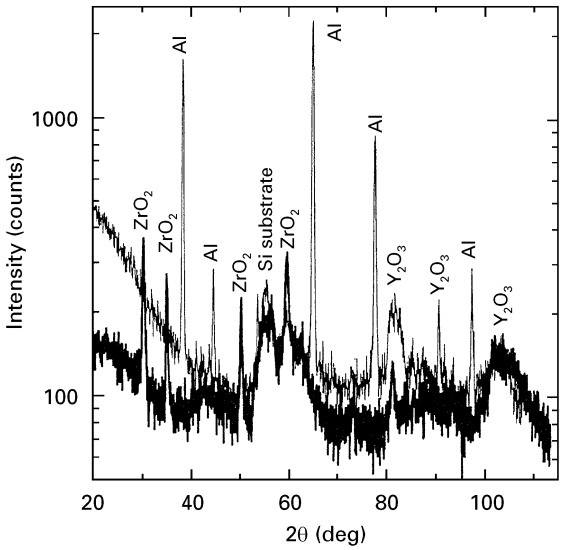

Figure 2 Diffraction patterns taken at an incidence angle of 0.5° on the film deposited at 830 °C before (thick line) and after (thin line) electrical conductivity measurements. The Al maxima come from the electrical contacts.

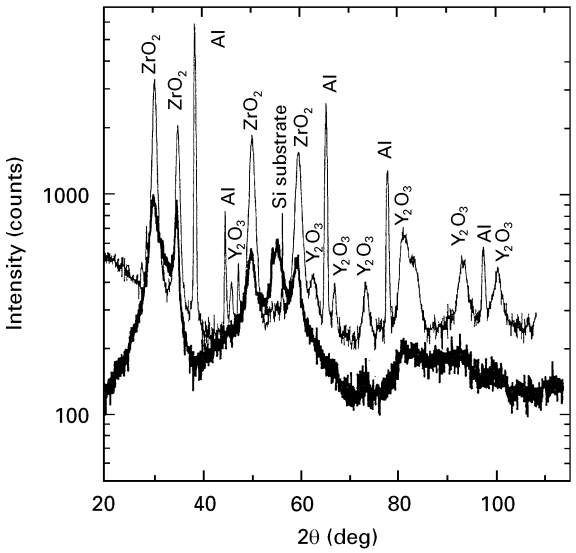

Figure 3 Diffraction patterns taken at an incidence angle of 0.5° on the film deposited at r.t. before (thick line) and after (thin line) electrical conductivity measurements. The Al maxima come from the electrical contacts.

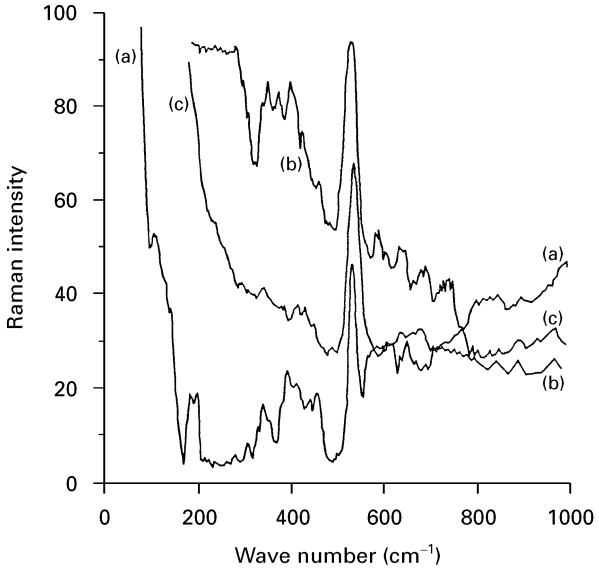

Figure 4 Raman spectra of thin YSZ films deposited on Si substrate at different temperatures. (a) r.t., (b) 700 °C and (c) 830 °C.

phase of Y_2O_3 (the strongest one was 8 4 4) were found in Fig. 2. The structure of the film with the best developed f.c.c. structure, deposited at 700 °C, was unchanged after such thermal treatment.

The mentioned effect of post-deposition thermal treatment of films on their structure is in good agreement with the behaviour of their electrical conductivity (Section 3.3).

The phase composition of the investigated films was also studied by Raman spectroscopy, which is very sensitive to the zirconia polymorphs. Typical spectra of the deposited films are shown in Fig. 4. As can be seen in this figure, both films with developed structure (700 and 830 °C) show only the cubic phase with no evidence of residual tetragonal or monoclinic zirconia, and are in agreement with the XRD investigation. The phase composition of the films was also verified by means of i.r. transmission measurements (Section 3.2).

3.2. I.r. transmission measurements

The measured spectra of films deposited at r.t. and 700 °C and the Si substrate only are shown in Fig. 5. In the spectrum of film deposited at 830 °C, an overall drop in the transmittance by 10–15% in the whole spectral range was observed, indicating a deterioration of the quality of the substrate. Therefore, this spectrum was not evaluated.

The spectra of the other two films (deposited at r.t. and 700 °C) were evaluated in the following way: the YSZ film transmittance T(YSZ), was determined as the ratio, $\tilde{T}(\text{YSZ}) = \tilde{T}(\text{Si substrate + YSZ})/\tilde{T}(\text{Si substrate})$; then $\tilde{T}$(YSZ), was fitted using a model of a single-oscillator dielectric function

$$\varepsilon(\omega) = \varepsilon_\infty + \Delta\varepsilon\omega_0^2/(\omega_0^2 - \omega^2 + i\gamma\omega)$$

where ε_∞ was the permittivity at high frequencies, $\Delta\varepsilon$ the contribution of oscillator to the dielectric permittivity, ω_0 the resonance frequency, and γ the damping. Model $\tilde{T}$(YSZ) was calculated from $\hat{\varepsilon}$ as the transmittance of a thin film using the formula taking into account the interference of beams multiply reflected within the film. The fitting parameters used are listed in Table I. In the last line of Table I, the parameters from [11] are shown, obtained as a fit of reflectance of a 20 wt % YSZ bulk sample. The authors simulated the spectra with two more oscillators, which are not listed in Table I. However, we have omitted these two oscillators in our fit, since their oscillator strength were much smaller than that of the main band.

The disagreement between the $\Delta\varepsilon$ parameters in the films and bulk sample may be caused by the simplified evaluation procedure used here, which neglects the interference effects within the substrate. The advantages of the approach used are its simplicity and the fact that it is not necessary to model the substrate spectrum, which is biased by diffraction on the surface of the substrate.

Conclusions about the properties of the YSZ film can be made on the basis of comparison of γ and ω_0 parameters with the bulk values. The large value of the γ (r.t.) parameter of the film deposited at r.t. indicates a high degree of amorphous state in the film. This is apparently also the cause of the shift of ω_0 (r.t.) parameter by 50 cm^{-1} with respect to the bulk value. By contrast, γ and ω_0 of the film deposited at 700 °C are close to the bulk value. This fact confirms unambiguously that this film is crystalline (f.c.c.). The small increase in ω_0 and γ still present in this sample as compared with the bulk values can be accounted for by small inhomogeneities due to possible strains in the film.

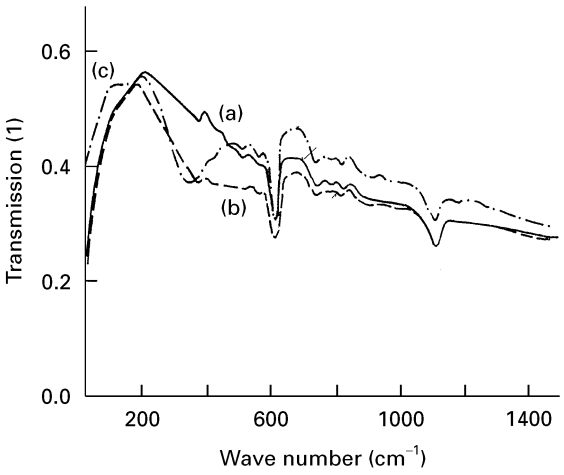

Figure 5 Smoothed i.r. transmission spectra of YSZ films deposited on Si substrate: (a) Si substrate, (b) YSZ film deposited at r.t., and (c) YSZ film deposited at 700 °C.

TABLE I Polar phonon parameters from the fit of YSZ thin films

Film	ε_∞	$\Delta\varepsilon$	ω_0 (cm^{-1})	γ (cm^{-1})
Deposited at r.t.	4.8	7.2	385	250
Deposited at 700 °C	4.8	5.5	346	120
Bulk material [11]	4.8	10.8	335	90

3.3. Electrical conductivity

The electrical conductivity was measured by a complex impedance method as a function of temperature of the cell

$$(-)\ \text{air, Al/YSZ/Si/Au, air}\ (+)$$

Fig. 6 shows a typical impedance diagram of a film deposited at 700 °C and taken at $T = 349$ °C. The total impedance of the investigated sample, i.e. the YSZ film deposited on Si substrate, consists of the impedance of the investigated YSZ film as well as the impedance of the Si substrate. However, as can be seen in Fig. 7 (Si, taken at 364 °C), the impedance contribution of the Si substrate alone, to the total impedance of the investigated sample is at least 100 times lower than that of the YSZ film. Therefore, the contribution of the impedance of the Si substrate was neglected during analysis of the data obtained. The electron beam evaporation-deposited films are characterized by only one arc due to the bulk conductivity $\sigma_b = K/R_b$ (Fig. 6), where K is the cell constant and R_b is the bulk resistance. The absence of grain boundary contributions in the investigated films, which are expected for the polycrystalline samples, can be explained by the purity of the powder and/or the relatively high density of the films due to the preparation conditions. This absence was confirmed also by other authors (e.g. [12, 13]) and not only for the films

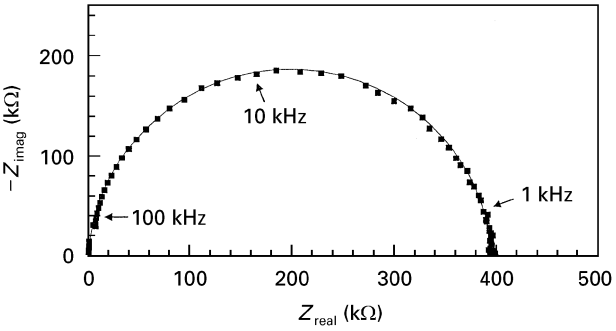

Figure 6 Complex impedance, Z, diagram of YSZ film deposited on Si substrate at 700 °C and taken at 349 °C.

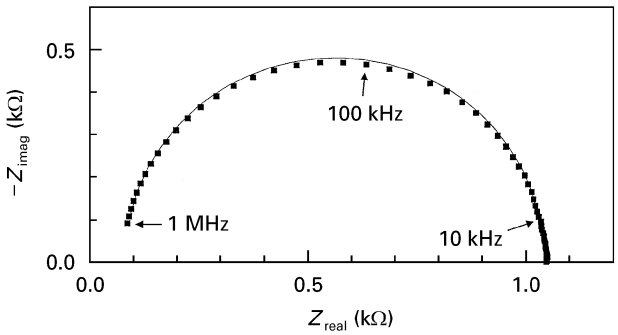

Figure 7 Complex impedance, Z, diagram of Si substrate taken at 364 °C.

prepared by the technique considered in this paper. The measurements were analysed according to the method of electrical equivalent circuit [14].

Arrhenius plots of the films deposited at different temperatures of the substrate (r.t., 700 and 830 °C) are shown in Fig. 8. According to the general expression

$$\sigma = A \times \exp(-E_a/kT) \quad (2)$$

the activation energies, E_a, obtained in the temperature region below 560 °C from the plots of log σ versus $1/T$ using the least squares method are presented in Fig. 8. In general, two straight line portions with different slopes are observable in the temperature dependence of conductivity for YSZ samples (e.g. [15]). This dependence of activation energy, E_a, on temperature is generally explained with the formation of dopant cation–vacancy pairs at low temperatures (< 600 °C). In this lower temperature region as in our case, the microstructure, impurity level and association phenomena are important.

The deposited films exhibit bulk conductivity very similar to that of YSZ films obtained by other techniques, e.g. plasma-spraying and sputtering deposition techniques and also with respect to the sintered and single crystal samples of the same composition (see e.g. [12, 13]). This similarity is a strong indication that the bulk conductivity of the film is also essentially ionic.

The activation energies, E_a, from 0.91 to 1.0 eV are also in good agreement with the data obtained on single crystals and sintered samples [12, 16].

The high concentrations of Y_2O_3 stabilizer used result in the partial presence of a Y_2O_3 secondary phase before the conductivity measurements are made, as mentioned in Section 3.1. The repeated measurements of conductivity (cycles of heating and cooling in the temperature range of r.t. – 560 °C) cause the precipitation of Y^{3+} ions from the YSZ lattice, i.e. the growth of a Y_2O_3 secondary phase. In such a way, the conductivity of the films decreases due to the decreasing amount of oxygen vacancies (charge carriers), which are present in the YSZ film in order to maintain electrical neutrality after the addition of Y_2O_3 into ZrO_2. This fact, together with the observed "softening" (the decrease of the amount of f.c.c. phase) of the film deposited at 830 °C (Fig. 1c), contribute to the observed decrease of conductivity of this film (Fig. 9). In contrast, the conductivity of the film deposited on the substrate at r.t. increases with repeated cycles of heating and cooling at the conductivity measurements (Fig. 10) due to the increasing conductive f.c.c. phase in this film (Fig. 3). The conductivity of the YSZ film deposited on the substrate at 700 °C was unchanged, similarly its structure, by the post-deposition thermal treatment.

3.4. Charge trapping at the YSZ–Si interface

To assess the quality of the YSZ–Si interface, charge DLTS [17] and feedback charge capacitance–voltage measurements [18] were conducted. The YSZ–Si deposition temperature has been found to play a significant role in the accessible sweep of the surface potential, Φ_s. Charge DLTS response of interface states in the small-signal regime (probing pulse $\Delta U = 0.1$ V) comprised a quasi discrete peak that changed its energy (temperature at maximum, T_m), with varying quiescent bias, as long as we dealt with YSZ films deposited at 700 °C (Fig. 11) or 830 °C

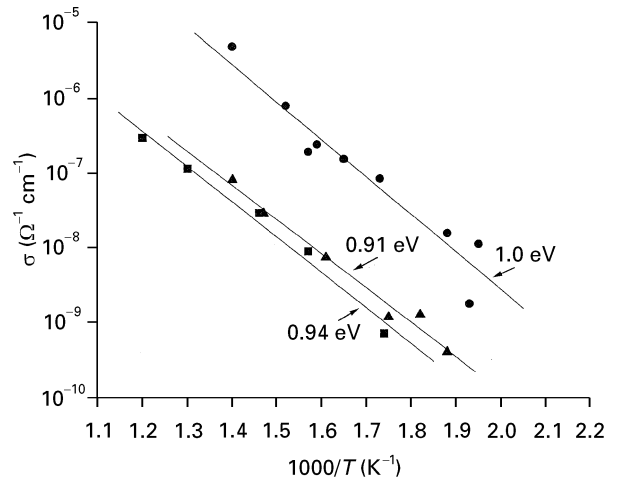

Figure 8 Arrhenius plots of conductivity versus temperature of YSZ films deposited on Si substrate at (■) r.t., (▲) 700 °C, and (●) 830 °C.

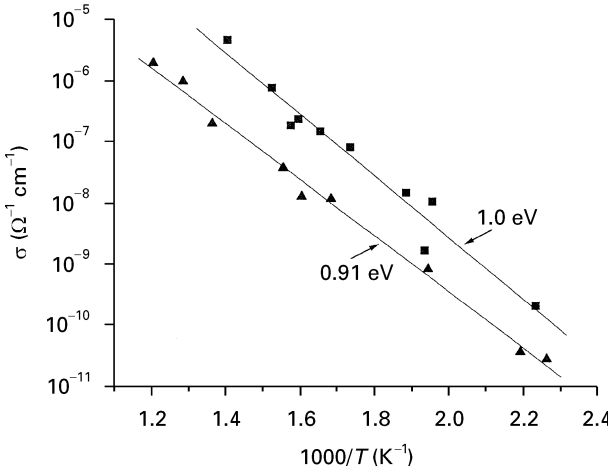

Figure 9 Arrhenius plots of conductivity versus temperature of YSZ film deposited on Si substrate at 830 °C measured on the as-prepared film (■) and on the film after its post-deposition thermal treatment (▲).

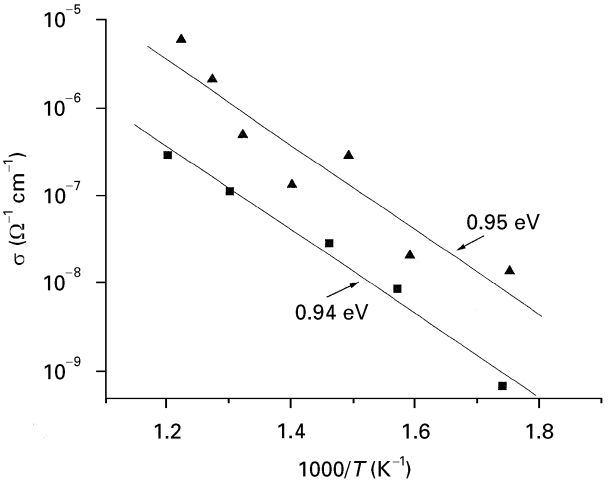

Figure 10 Arrhenius plots of conductivity versus temperature of YSZ film deposited on Si substrate at r.t. measured on the as-prepared film (■) and on the film after its post-deposition thermal treatment (▲).

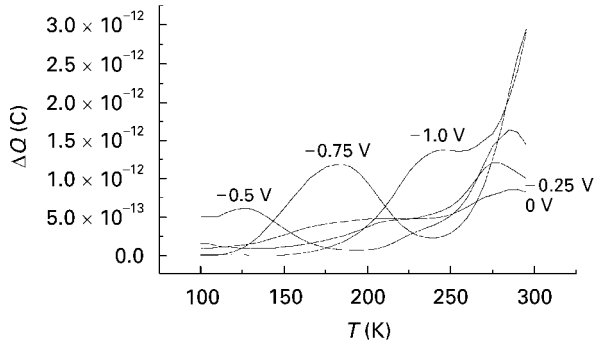

Figure 11 Charge DLTS spectra of an MIS structure with a YSZ insulator deposited at 700 °C at different quiescent gate biases, U_g: the high-temperature tail ($U_g < -0.75$ V) is due to minority carrier generation under a weak inversion. The rate window corresponds to sampling events at time, $t_1 = 1$ ms and $t_2 = 2$ ms, respectively.

(Fig. 12), respectively. Yet, the structures deposited at 700 °C exhibited the highest $\Delta\Phi_s/\Delta U_g$ ratio and could be driven to accumulation even at 90 K, compared with those deposited at 830 °C that remained in deep depletion at low temperatures and forward (positive) gate biases. We have concluded, therefore, that the density of YSZ–Si interface states is a minimum when a cubic YSZ is interfaced with the crystalline n–Si. The hysteresis of related feedback charge C–V curves evident from Fig. 13 can be reconciled with oxygen vacancies movements in the insulator even at ambient temperatures, keeping in mind that after negative biasing there is an excess negative charge at the YSZ–Si interface. The same behaviour of the flatband voltage shift has been reported earlier for C–V data obtained by means of alternating current (a.c.) techniques [19, 20]. Finally, on considering an MIS structure with a YSZ insulator deposited at r.t. the corresponding DLTS spectra were dominated by a discrete energy level (at a well defined T_m) that pinned the surface potential within the 90–300 K range, the complementary feedback charge capacitance did not change with gate bias, as expected.

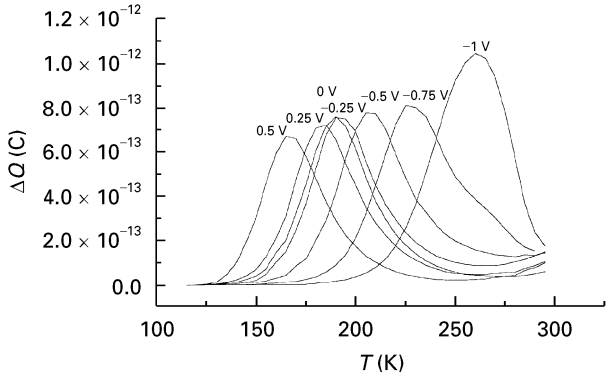

Figure 12 Charge DLTS response of an MIS device with a YSZ insulator deposited at 830 °C, the sampling regime being the same as defined for Fig. 11. Onset of inversion is now at $U_g = -1$ V.

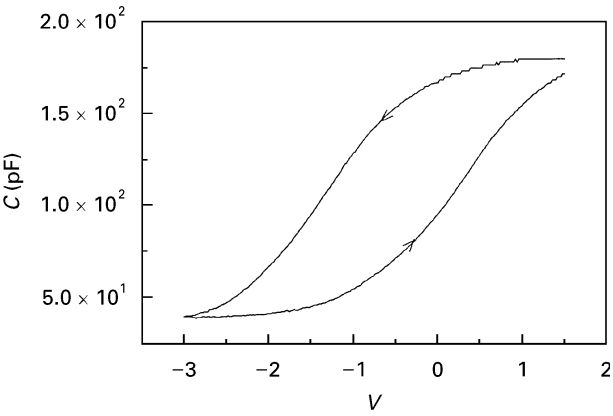

Figure 13 Feedback charge capacitance of the sample from Fig. 12 as a function of gate bias, the capacitance was taken after 3 μs with respect to the bias step $\Delta U = 0.06$ V.

4. Conclusions

YSZ films were deposited by means of electron beam evaporation on n-doped Si(1 0 0) substrates at three different temperatures (r.t., 700 and 830 °C). The structure was found to change from essentially amorphous YSZ at r.t. through the best developed cubic fluorite-type structure at 700 °C, up to a cubic phase combined with an amorphous one at 830 °C with a lattice parameter of 0.5184 nm and an average grain size of about 24.5 nm. The composition of the phase was verified by means of Raman spectroscopy and by i.r. transmission measurements. There was no evidence for the presence of tetragonal or monoclinic zirconia. Similarly, no interfacial as well as no zirconate phases were detected neither before the electrical measurements nor after five cycles of conductivity measurements (up to 560 °C). The high concentration of the stabilizer used ($\sim$30 mol % Y_2O_3 or $\sim$20 mol % $YO_{1.5}$) caused part of the Y^{3+} ions to be present in the form of Y_2O_3 phase before conductivity measurements; the repeated cycles of conductivity measurements resulted in a still higher amount of Y^{3+} ions present in the secondary phase Y_2O_3, as was confirmed by the conductivity measurements.

The ionic conductivity and activation energy (0.91–1.0 eV) of the deposited films were very similar to those of YSZ bulk material, but no grain boundary effect was observed in the films.

The charge DLTS and feedback charge capacitance–voltage measurements performed showed that the YSZ–Si deposition temperature played an important role in the accessible sweep of the surface potential Φ_s. The C–V characteristics of the MIS structures incorporating YSZ films measured at r.t. showed hysteresis and positive shifts of the flatband voltages. The hysteresis has been considered to be due to the movement of oxygen vacancies in the film.

Acknowledgements

The work was partially supported by the research grants No. 2/1004/96, 2/1172/96, 2/1165/96 and 1/1379/94 of the Slovak Grant Agency and No. A 1010507 of the Grant Agency of the Czech Academy of Sciences.

References

1. H. S. ISAACS, *Adv. Ceram.* **3** (1981) 406 and references therein.
2. G. VELASCO, *Solid State Ionics* **9**/**10** (1983) 783.
3. S. CHANDRA, in "Superionic Solids" (North Holland, Amsterdam, 1981) Ch. 6 and references therein.
4. J. A. KILNER and B. C. H. STEELE, in "Non-stoichiometric oxides", edited by O. T. Sorensen (Academic, London, 1981) p. 233.
5. M. J. VERKERK, A. J. A. WINNUBST and A. J. BURGGRAAF, *J. Mater. Sci.* **17** (1982) 3113.
6. S. BADWAL, *ibid.* **19** (1984) 1767.
7. S. CHROMIK, B. WUYTS, I. VÁVRA, A. ROSOVÁ, F. HANIC, S. BEŇAČKA and Y. BRUYNSERAEDE, *Physica C* **226** (1994) 153.
8. T. MATTHEE, J. WECKER, H. BEHNER and G. FRIEDEL, *J. Appl. Phys. Lett.* **61** (1992) 1240.
9. I. THURZO and K. GMUCOVÁ, *Rev. Sci. Instrum.* **65** (1994) 2244.
10. B. E. WARREN, in "X-ray diffraction" (Addison-Wesley, Reading, MA, 1969).
11. D. W. LIU, C. H. PERRY and R. P. INGEL, *J. Appl. Phys.* **64** (1988) 1413.
12. G. CHIODELLI, A. MAGISTRIS, M. SCAGLIOTTI and F. PARMIGIANI, *J. Mater. Sci.* **23** (1988) 1159.
13. C. C. CHEN, M. M. NASRALLAH and H. U. ANDERSON, *Solid State Ionics* **70**/**71** (1994) 101.
14. B. A. BOUKAMP, "Equivalent circuit (EQUIVCRT. PAS) users manual" (University of Twente, Department of Chemical Technology, The Netherlands, 1989).
15. T. NORBY and M. HARTMANOVÁ, *Solid State Ionics* **67** (1993) 57.
16. M. HARTMANOVÁ, I. TRAVĚNEC, A. A. URUSOVSKAYA, K. PUTYERA, D. TUNEGA and I. I. KOROBKOV, *ibid.* **76** (1995) 207.
17. J. W. FARMER, C. D. LAMP and J. M. MEESE, *J. Appl. Phys. Lett.* **41** (1982) 1063.
18. T. J. MEGO, *Rev. Sci. Instrum.* **57** (1986) 353.
19. P. E. BAGNOLI, C. CIOFI, A. DILIGENTI, A. INNAMORATO and A. NANNINI, *Thin Solid Films* **264** (1995) 109.
20. Y. MIYAHARA, *J. Appl. Phys.* **71** (1992) 2309.

Received 18 December 1996
and accepted 1 September 1997